Stem Cell Reports
Article

OPEN ACCESS

Differential Maturation of the Two Regulated Secretory Pathways in Human iPSC-Derived Neurons

Javier Emperador Melero,[1] Aishwarya G. Nadadhur,[1] Desiree Schut,[1] Jan V. Weering,[1] Vivi M. Heine,[1,2,3] Ruud F. Toonen,[1,*] and Matthijs Verhage[1,*]

[1]Departments of Functional Genomics and Clinical Genetics, Center for Neurogenomics and Cognitive Research, Amsterdam Neuroscience, Vrije Universiteit (VU) Amsterdam and VU Medical Center, de Boelelaan 1087, 1081 HV Amsterdam, the Netherlands
[2]Department of Pediatrics/Child Neurology, Amsterdam Neuroscience, VU Medical Center, 1081 HV Amsterdam, the Netherlands
[3]Department of Complex Trait Genetics, Center for Neurogenomics and Cognitive Research, Amsterdam Neuroscience, Vrije Universiteit Amsterdam, 1081 HV Amsterdam, the Netherlands
*Correspondence: ruud.toonen@cncr.vu.nl (R.F.T.), matthijs@cncr.vu.nl (M.V.)
http://dx.doi.org/10.1016/j.stemcr.2017.01.019

SUMMARY

Neurons communicate by regulated secretion of chemical signals from synaptic vesicles (SVs) and dense-core vesicles (DCVs). Here, we investigated the maturation of these two secretory pathways in micro-networks of human iPSC-derived neurons. These micro-networks abundantly expressed endogenous SV and DCV markers, including neuropeptides. DCV transport was microtubule dependent, preferentially anterograde in axons, and 2-fold faster in axons than in dendrites. SV and DCV secretion were strictly Ca^{2+} and SNARE dependent. DCV secretion capacity matured until day in vitro (DIV) 36, with intense stimulation releasing 6% of the total DCV pool, and then plateaued. This efficiency is comparable with mature mouse neurons. In contrast, SV secretion capacity continued to increase until DIV50, with substantial further increase in secretion efficiency and decrease in silent synapses. These data show that the two secretory pathways can be studied in human neurons and that they mature differentially, with DCV secretion reaching maximum efficiency when that of SVs is still low.

INTRODUCTION

Neurons communicate primarily by regulated secretion of signaling molecules via two secretory pathways, using synaptic vesicles (SVs) and using dense-core vesicles (DCVs). SVs contain neurotransmitters responsible for fast signaling (Kaeser and Regehr, 2014; Rizo and Sudhof, 2012; Sudhof and Rothman, 2009), whereas DCVs store neuromodulators such as neuropeptides and neurotrophins that regulate brain development, synaptogenesis, and synaptic plasticity (Huang and Reichardt, 2001; Park and Poo, 2013; van den Pol, 2012; Zaben and Gray, 2013). While SVs recycle locally in nerve terminals, DCVs are filled with cargo at the *trans*-Golgi network (TGN). After post-Golgi maturation (Kim et al., 2006), DCVs are transported by microtubule-linked motor proteins to specific fusion sites (de Wit et al., 2006; Maeder et al., 2014), where they secrete their cargo upon high-frequency stimulation (HFS) (Farina et al., 2015; Shimojo et al., 2015; van de Bospoort et al., 2012). Currently, insight into these regulated secretory pathways comes mostly from rodent neuronal cultures, invertebrates, or human immortalized cell lines, but validation of such insight in human, post-mitotic neurons is currently lacking, despite new opportunities to do so using human induced pluripotent stem cell (iPSC)-derived neurons.

Human iPSC-derived neurons provide new tools to model human brain disorders, test therapeutic targets on a patient-own background, and conduct translational studies (Ichida and Kiskinis, 2015). Dysregulation of the regulated secretory pathways is evidently linked to many brain disorders, including post-traumatic stress disorder, cognitive impairment (Meyer-Lindenberg et al., 2011; Sah and Geracioti, 2013), schizophrenia, autism, or intellectual disability (Volk et al., 2015). Studies on regulated secretory pathways in human iPSC-derived neurons will be important to better understand the etiology of these disorders. Several recent studies have demonstrated that SV secretion is functional in human neurons, using postsynaptic recordings in synaptic networks of human neurons. However, surprisingly few studies (such as Chanda et al., 2014; Sun et al., 2016; Yi et al., 2016; Zhang et al., 2013) have reported evoked secretion, which is the basis for synaptic transmission, and most studies only report spontaneous fusion of SVs, of which the biological significance is unclear. For trafficking and secretion of DCV cargo, such as neuropeptides and neurotrophic factors, even fewer studies have been conducted in human neurons and these ones provide limited resolution of the secretion process (Hook et al., 2014; Merkle et al., 2015). Hence, the characterization of secretory pathways in human iPSC-derived neurons remains limited and it is unclear to what extent human neurons model mature secretory pathways in the brain, a prerequisite to investigate human brain disorders.

In this study, we investigated the development of both regulated secretory pathways in human iPSC-derived neurons using electron microscopy, and live and confocal imaging. We show that human iPSC-derived neurons express endogenous SV markers and DCV cargo. We developed

quantitative assays to monitor DCV trafficking and secretion at single-vesicle resolution and study activity-dependent SV secretion. We show that the secretion efficiency of the two pathways develops differentially, with DCVs acquiring maximal secretion efficiency when that of SVs is still low.

RESULTS

Human iPSC-Derived Neurons Express Endogenous DCV and SV Markers

To assess regulated secretion in human neurons, we generated mixed networks of excitatory and inhibitory neurons (Figures 1A and 1B), with around 40% GABAergic neurons (Figures 1C and 1D), following a standard differentiation procedure (Ma et al., 2012) with minor modifications. These neurons were seeded onto glia islands to form micro-networks of four to ten neurons (Figures 1E and 1F). We first investigated the presence of SVs and DCVs in these networks at 50 days in vitro (DIV). DIV14 mouse hippocampal neurons were included as a well-characterized reference model.

SV markers synaptobrevin-2 and synaptophysin were expressed as discrete puncta on dendrites of human neurons (Figures 2A, 2D, S1A, and S1C) similar to synaptophysin in mouse neurons (Figures S1B and S1D). We also found strong expression of the DCV markers neuropeptide-Y (NPY) and chromogranin-B (CgB) in these cultures (Figures 2B and 2C). Both NPY and CgB were expressed as discrete puncta (Figures 2E and 2F), similar to mouse neurons (Figures S1E–S1H). NPY expression was restricted to a subset of neurons (Figure 2B) in line with cultures of mouse neurons (Figure S1E) and its expression profile in vivo (Allen et al., 1983).

We next quantified the density of SV and DCV puncta using semi-automated immunofluorescence detection (Figures 2G and 2H; Schmitz et al., 2011). The average density of SV markers in human iPSC-derived neurons was 0.12 per μm of neurite, almost 30% lower than in mouse neurons (Figure 2I), while NPY or CgB puncta appeared at an average density of 0.4 per μm of neurite, similar to mouse neurons (Figure 1J; van de Bospoort et al., 2012). Together, the punctate pattern of DCV and SV markers suggests that human iPSC-derived neurons contain DCV and SV clusters at DIV50.

To confirm that these puncta of DCV and SV markers are indeed DCV and SV clusters, we performed electron microscopy. We identified asymmetric and en-passant synaptic structures with SVs clustered at the presynaptic active zone (Figures 2K and S2B–S2F). In addition, we also observed areas where SVs started to cluster in the proximity of the plasma membrane (Figures S2A and S2D). DCVs were present in synaptic terminals (Figure 2K) and neurites (Figure 2L). The average SV and DCV diameters was 35 and 75 nm, respectively (Figures 2M and 2N), comparable with mouse neurons (van de Bospoort et al., 2012).

Together, these results confirm the presence of DCVs, SV clusters, and synapses in these human neurons. Furthermore, self-organizing principles that diversify neuronal identity in the developing brain seem to be, at least partially, recapitulated in vitro as suggested by the strong NPY expression in a subset of neurons.

DCV Trafficking Is Microtubule Dependent and Differs between Axons and Dendrites in Human iPSC-Derived Neurons

We next characterized DCV trafficking in human iPSC-derived neurons at DIV50. To do so, we expressed an established DCV cargo-reporter, NPY-mCherry (de Wit et al., 2009; Farina et al., 2015), via lentiviral infection. This protein showed a punctate pattern typical of DCVs (Figures 3A and S3A). Ninety percent of the signal of this reporter co-localized with the endogenous DCV cargo, CgB (Figures S3B and S3C). NPY-mCherry puncta were present in axons and dendrites (Figure 3A). We observed moving and stationary DCV puncta (Figure 3B). Moving DCV puncta showed anterograde, retrograde, and bidirectional movement with or without pausing times. DCV trafficking in axons was faster than in dendrites (Figures 3B and 3C; Movie S1), with average axonal speed reaching 1 μm/s for anterograde and 0.6 μm/s for retrograde transport, while in dendrites the average speed was 0.4 μm/s for both directions (Table 1). Peak velocities reached 3.5 and 1.5 μm/s in axons and dendrites, respectively (Figure 3C). Furthermore, anterograde trafficking was preferential in axons (36% of all puncta, Table 1) whereas in dendrites, most puncta moved bidirectionally or remained stationary (30% for each, Table 1). Similar trafficking dynamics were observed at an earlier developmental stage (DIV24, Table 1).

DCV trafficking depends on polymerized microtubules in rodent neurons (Hirokawa et al., 2010; Vale, 2003). To test this in human neurons, we disrupted microtubule polymerization by acute incubation with nocodazole (10 μM for 45 min, Figure 3D), which resulted in robust reduction in βIII-tubulin intensity, as expected (Figure 3E). This disruption strongly affected DCV trafficking, resulting in 85% and 75% reduction in average speed in axons and dendrites, respectively (Figures 3F and 3G; Movie S1), and increased pausing time (by 80% and 55% in axons and dendrites, respectively, Figure 3H).

These results show that DCV trafficking in human neurons is microtubule dependent and that trafficking dynamics differ between axons and dendrites, with axons specializing in fast, anterograde transport, in line with observations in mouse neurons (de Wit et al., 2006; Kwinter et al., 2009).

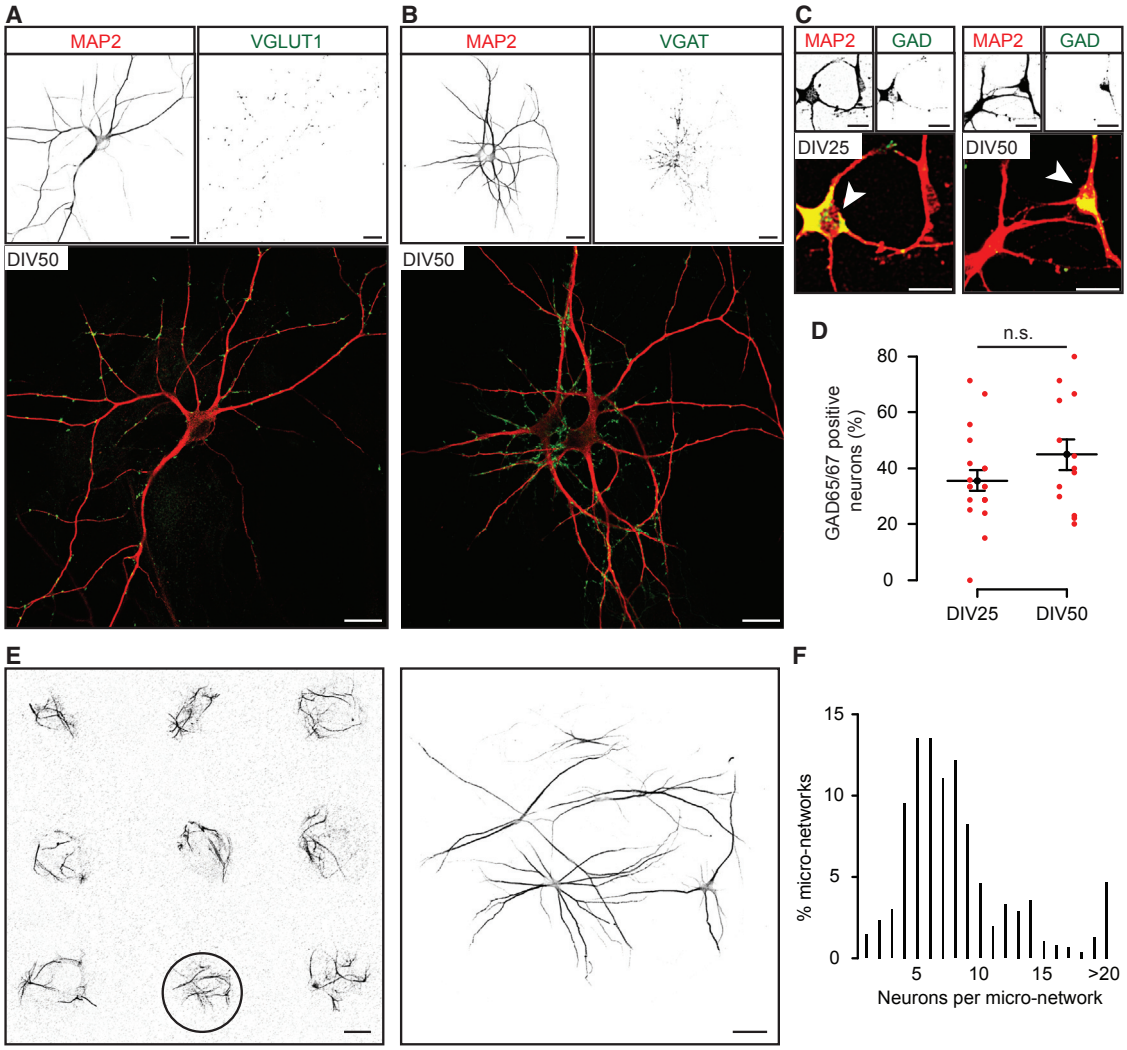

Figure 1. Micro-Networks of Excitatory and Inhibitory Human iPSC-Derived Neurons

(A and B) Representative images of DIV50 human iPSC-derived neurons immunostained for MAP2 and excitatory (VGLUT1) (A) or inhibitory (VGAT) (B) synaptic vesicle proteins.

(C) Representative images of DIV25 or DIV50 human iPSC-derived neurons immunostained for MAP2 and the GABAergic marker GAD65/67. Arrowheads indicate positive GAD65/67 neurons.

(D) Percentage of GAD65/67-positive neurons remains constant from DIV25 to DIV50 (DIV25: 35.63% ± 3.66%, n = 20; DIV50: 44.92% ± 5.57%, n = 13 images from two independent inductions; p = 0.155). Images with less than four neurons were excluded. n.s., not significant.

(E) Overview of MAP2-stained DIV50 human iPSC-derived neurons grown on astrocyte-based micro-networks (left) and zoom (black circle) of a typical micro-network (right).

(F) Histogram of the number of human iPSC-derived neurons per micro-network. N = 450 micro-networks from three independent inductions.

Scale bars, 20 μm (A–D); 100 μm (E), overview; and 40 μm (E), zoom.

Secretion of DCVs and SVs in Human iPSC-Derived Neurons Occurs upon HFS in a Calcium and SNARE-Dependent Manner

Secretion of SVs is driven by the formation of *trans*-SNARE complexes consisting of synaptobrevin-2, SNAP25, and syntaxin1, in coordination with other proteins such as Munc-18-1, in a calcium-dependent manner (Kaeser and Regehr, 2014; Rizo and Sudhof, 2012; Sudhof and Rothman, 2009). Similar principles are expected to operate for DCVs (de Wit et al., 2009; Shimojo et al., 2015). These proteins are abundantly expressed in glutamatergic and GABAergic human iPSC-derived neurons (Figures 2A and

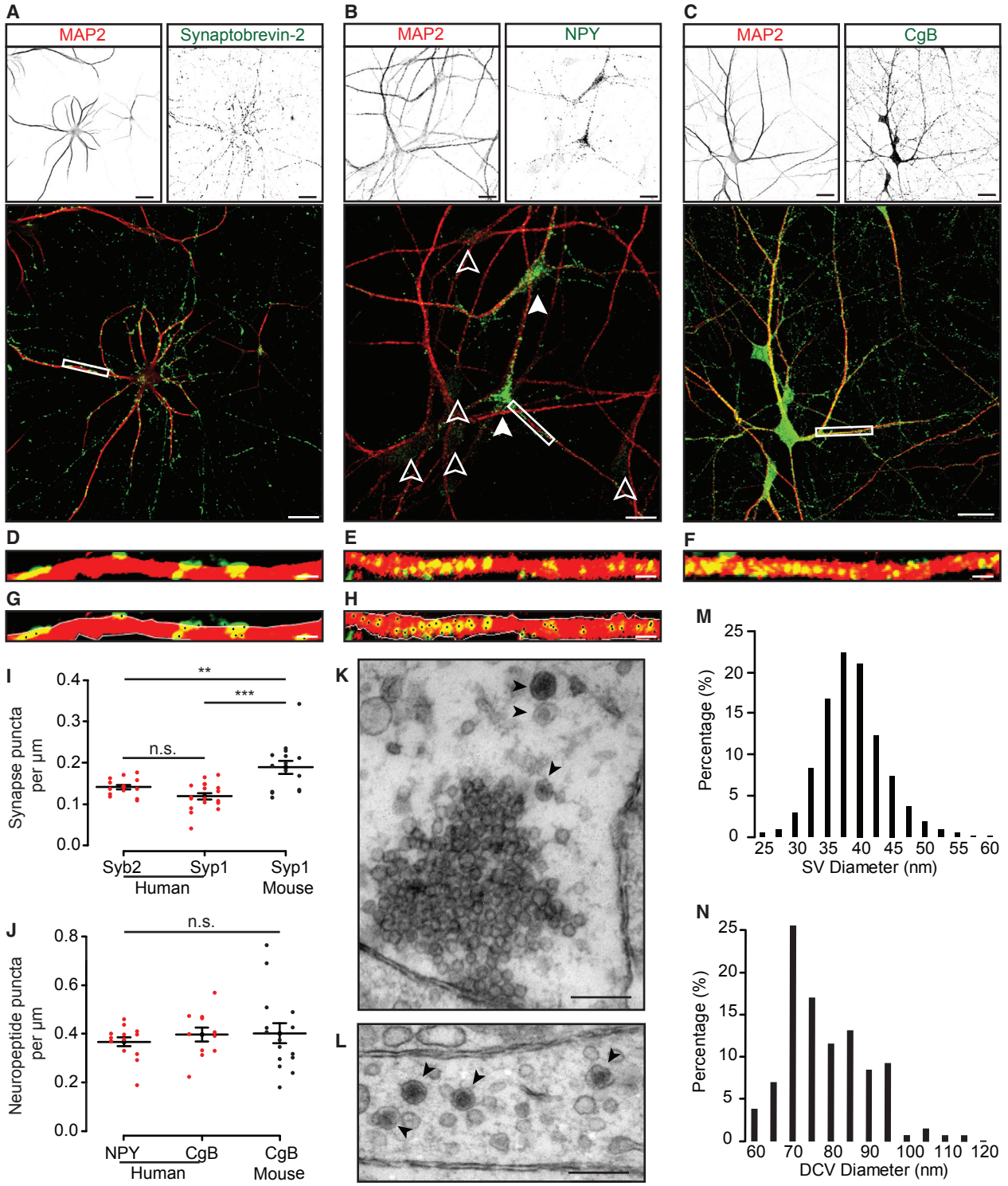

Figure 2. Human iPSC-Derived Neurons Express Endogenous Dense Core and Synaptic Vesicle Markers

(A–F) Representative images and zooms (white rectangles) of DIV50 human iPSC-derived neurons immunostained for MAP2 and the SV protein synaptobrevin-2 (A) and (D) or the DCV markers neuropeptide-Y (NPY) (B) and (E), and chromogranin-B (CgB) (C) and (F). White and open arrowheads indicate positive or negative NPY neurons, respectively.

(legend continued on next page)

S4A–S4P). First, we tested whether SV secretion was indeed SNARE and calcium dependent in the micro-networks of human neurons. We expressed the SV transmembrane protein synaptophysin fused to a pH-sensitive fluorophore (pHluorin) in a luminal domain (SypHy; Granseth et al., 2006) in DIV50 human iPSC-derived neurons. SypHy is quenched at rest due to the luminal acidic pH of SVs. We applied a standard protocol (Figure 4A) of HFS consisting of 100 action potentials (AP) at 40 Hz to evoke SV secretion, followed by NH_4^+ superfusion. NH_4^+ neutralizes the luminal pH of SVs and the resultant increase in fluorescence was used to estimate the total SV pool per synapse. No fluorescence was observed before HFS, confirming that SVs were indeed acidic (Figure 4B, left column, Movie S2). HFS resulted in fluorescence appearance, indicating SV fusion (Figure 4B, middle column, Movie S2). Furthermore, NH_4^+ superfusion led to a robust increase of fluorescence (Figure 4B, right column, Movie S2).

To test SNARE dependence of SV secretion, we expressed tetanus neurotoxin (TeNT), which led to efficient cleavage of synaptobrevin-2 (Figure 4C). Reponses to HFS were abolished by synaptobrevin-2 cleavage (Figures 4D and 4E). Similarly, HFS did not trigger fluorescence changes in the absence of extracellular calcium (Figures 4F and 4G). These data show that SV fusion depends on calcium and functional SNARE proteins in DIV50 human iPSC-derived neurons.

Second, a similar strategy was used to study SNARE and calcium dependence of DCV secretion, applying a stimulation protocol (16 bursts of 50 AP at 50 Hz, Figure 4H) known to trigger robust DCV secretion in mouse neurons (Farina et al., 2015; van de Bospoort et al., 2012). We first confirmed DCV acidity by expression of pHluorin fused to the DCV cargo protein NPY (Figure S5). Then, we substituted pHluorin for mCherry (Figure 4I), which is much less sensitive to pH and allows analysis of DCV dynamics and secretion. We observed efficient secretion, characterized by sudden disappearance of NPY-mCherry fluorescence, and of stationary and moving DCVs (Figure 4J; Movie S3), along with sharp increase in the intracellular calcium concentration (Figure 4K). As expected, the same stimulation protocol did not increase intracellular calcium and triggered no DCV secretion in the absence of external calcium (Figures 4K and 4L). Neurons expressing TeNT or control plasmid were identified by expression of soluble mCherry and therefore DCVs were labeled with NPY-GFP instead of NPY-mCherry (Figure 4M). TeNT expression inhibited DCV secretion in human iPSC-derived neurons (Figure 4N).

These results indicate that DCV secretion, similar to SVs, is calcium and SNARE dependent in human iPSC-derived neurons.

Synaptic Transmission Increases between DIV22 and DIV50 in Maturing Human iPSC-Derived Neurons

After corroborating that secretion of DCVs and SVs in human iPSC-derived neurons is dependent on SNAREs and calcium, we investigated the development of these pathways in the micro-networks. We investigated SV secretion efficiency at five time points, between DIV22 and DIV50. As before, we included mouse neurons as a reference model of a well-characterized mammalian neurosecretory system. SypHy fluorescence was quenched at resting conditions and dequenched upon NH_4^+ at every developmental stage (Figures 5A and 5C; Movie S2), indicating that SypHy is targeted to SVs and that they are already acidic compartments at DIV22. However, the number of SypHy puncta was 6-fold higher at DIV50 than DIV22 (Figures 5A and 5D), suggesting a robust increase in synapse formation between DIV22 and DIV50. HFS triggered SV secretion in some of these puncta. The percentage of non-responding (silent) synapses decreased 3-fold between DIV22 and DIV50 (Figure 5E). The percentage of silent synapses at DIV50 was not significantly different from mouse neurons (although a trend toward a lower percentage was observed: 35% and 20%, respectively, Figure 5E). The SypHy intensity upon $NH4^+$ superfusion also gradually increased almost 3-fold from DIV22 to DIV50 (Figure 5F) and, surprisingly,

(G and H) Representative output of the semi-automated quantification of SVs (G) and DCVs (H). White lines show morphological mask. Black dots indicate synapses (G) or DCVs (H) detected.

(I) The density of different SV markers remains constant in DIV50 human iPSC-derived neurons (synaptobrevin2 [Syb2]: 0.13 ± 0.01 puncta per μm, n = 11; synaptophysin1 [Syp1]: 0.11 ± 0.01 puncta per μm, n = 11, p = 0.124), but lower than mouse neurons (0.18 ± 0.01, n = 15; **p = 0.004, ***p = 3.1×10^{-5}, one-way ANOVA).

(J) The density of different DCV markers is similar in DIV50 human iPSC-derived neurons (NPY: 0.37 ± 0.02 puncta per μm, n = 13; CgB: 0.40 ± 0.03 puncta per μm, n = 11) and mouse neurons (CgB: 0.40 ± 0.04 puncta per μm, n = 15; p = 0.697, Kruskal-Wallis).

(K and L) Representative electron micrographs of DCVs (arrowheads) in synaptic terminals (K) and neurites (L) of DIV50 human iPSC-derived neurons.

(M) Histogram of SV diameters (average of 37.62 ± 0.14 nm, 1,253 SVs from 25 micrographs).

(N) Histogram of DCV diameters (average of 76.16 ± 1.00 nm, 130 DCVs from 53 micrographs).

Bars show mean ± SEM. Bullets and columns represent individual observations and inductions (nests for mouse), respectively. Scale bars, 20 μm (A–C); 2 μm (D–H); and 200 nm (K and L). See also Figures S1 and S2.

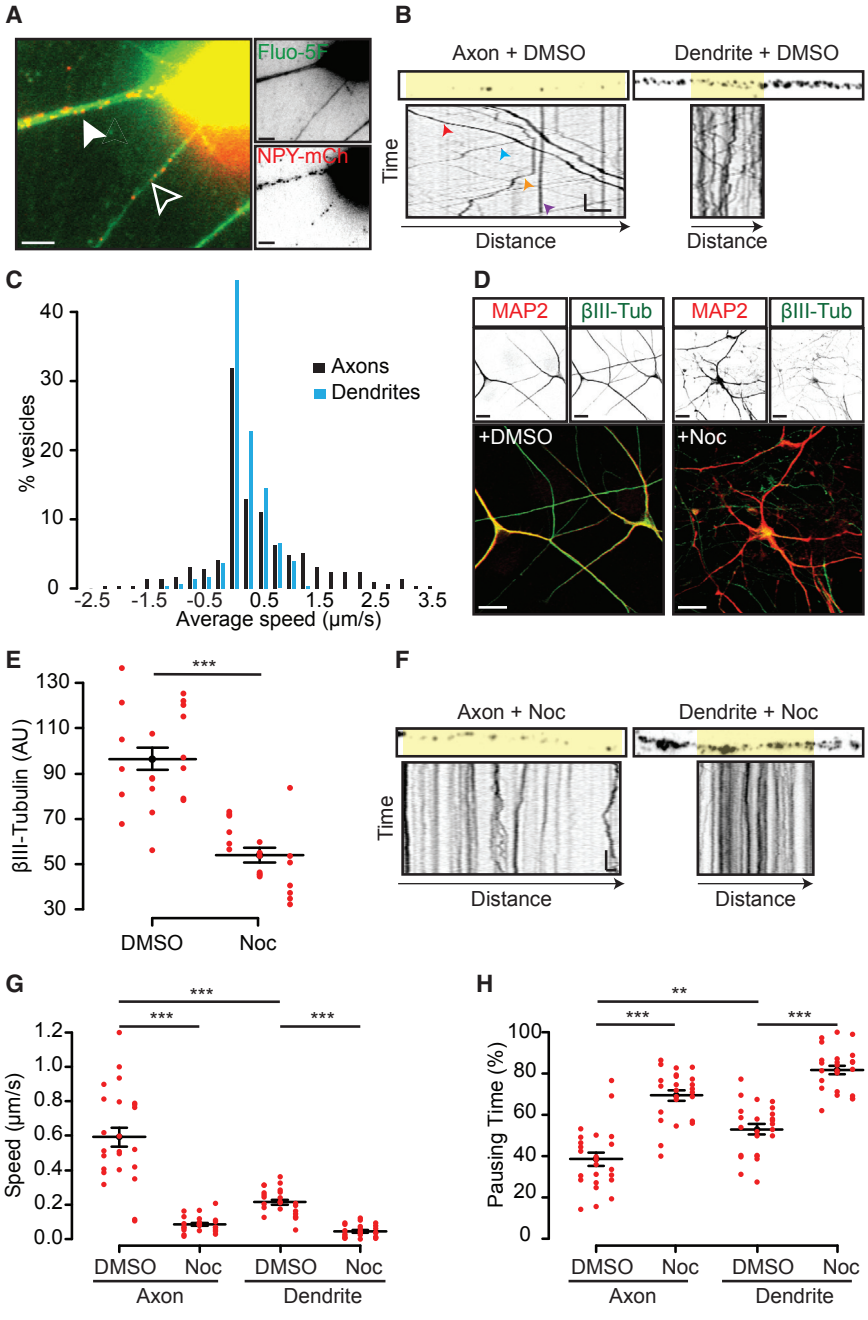

Figure 3. DCV Trafficking in Human iPSC-Derived Neurons Is Microtubule Dependent and Faster in Axons than Dendrites

(A) Representative NPY-mCherry-expressing human iPSC-derived neurons at DIV50 incubated with Fluo-5F. White and open arrowheads indicate dendrites (diameter >1.5 μm) and axons (<1 μm), respectively.

(B) Representative axon and dendrite containing NPY-mCherry puncta and corresponding kymograph (from yellow area). Red, blue, yellow, and purple arrowheads show examples of anterograde, retrograde, bidirectional trafficking, and stationary vesicles, respectively. Arrow indicates anterograde direction.

(C) Histogram of average DCV speed in dendrites and axons. Negative values indicate retrograde direction.

(D) Representative example of DIV50 human iPSC-derived neurons treated with nocodazole (10 μM in 0.1% DMSO) or DMSO and immunostained for MAP2 and βIII-tubulin.

(E) Nocodazole incubation decreases βIII-tubulin expression (DMSO: 96.48 ± 4.90 a.u., n = 20; Noc: 53.93 ± 3.12 a.u., n = 20; ***$p = 2.32 \times 10^{-8}$, Mann-Whitney U test).

(F) Representative axon and dendrite containing NPY-mCherry puncta and corresponding kymograph (from yellow area) showing trafficking arrest upon nocodazole treatment.

(G) DCV speed is higher in axons than dendrites (***$p = 1.8 \times 10^{-6}$) and reduced after nocodazole incubation in axons (DMSO: 0.59 ± 0.06 μm/s; Noc: 0.09 ± 0.01 μm/s, ***$p = 4.8 \times 10^{-8}$) and dendrites (DMSO: 0.21 ± 0.02 μm/s; Noc: 0.05 ± 0.01 μm/s, ***$p = 4.7 \times 10^{-8}$, Kruskal-Wallis).

(H) DCV pausing time is higher in dendrites than axons (**p = 0.003) and increased upon nocodazole incubation in axons (Noc: 69.33% ± 2.52%; DMSO: 38.48% ± 3.11%, ***$p = 3.0 \times 10^{-12}$) and dendrites (Noc: 81.70% ± 2.14%; DMSO: 52.91% ± 2.56%, ***$p = 3.5 \times 10^{-11}$, one-way ANOVA). Bars show mean ± SEM. Bullets and columns represent individual observations and inductions, respectively.

Scale bars, 5 μm (A); 20 μm (D); 5 μm and 10 s (B) and (F). For trafficking assays, n = 15–20 vesicles per neurite per micro-network. Twenty-four micro-networks analyzed per condition. See also Figure S3.

surpassed that of mouse neurons (3.89 and 2.33 a.u., respectively, Figure 5F). SV secretion showed a similar pattern of progressive increase, with a 7-fold increase from DIV22 to DIV50 (Figures 5G and 5H), remaining 2-fold below mouse neurons (0.26 and 0.55 a.u., respectively, Figures 5G and 5H). SV secretion efficiency, calculated as the ratio of fluorescence increase upon stimulation divided by the maximum fluorescence increase upon NH_4^+ superfusion, also increased from DIV22 to DIV50, but remained 3- to 4-fold lower than in mouse neurons (Figure 5I). A similar

Table 1. DCV Trafficking Dynamics in Human iPSC-Derived Neurons

	Speed (μm/s)			Percentage (%)		
	DIV24	DIV50 (DMSO)	DIV50 (Noc)	DIV24	DIV50 (DMSO)	DIV50 (Noc)
Axons						
Anterograde	0.94 ± 0.12	1.07 ± 0.11	0.16 ± 0.02	37.71 ± 3.81	36.29 ± 2.16	18.74 ± 2.72
Retrograde	0.88 ± 0.09	0.66 ± 0.08	0.10 ± 0.02	21.44 ± 3.01	21.86 ± 2.10	7.84 ± 1.71
Bidirectional	0.54 ± 0.07	0.48 ± 0.07	0.15 ± 0.01	18.97 ± 3.42	18.35 ± 2.15	28.36 ± 2.33
Stationary	–	–	–	21.88 ± 4.06	23.46 ± 2.59	45.06 ± 3.41
Dendrites						
Anterograde	0.59 ± 0.11	0.47 ± 0.06	0.09 ± 0.02	18.08 ± 2.06	18.87 ± 2.05	12.91 ± 1.95
Retrograde	0.47 ± 0.06	0.37 ± 0.07	0.07 ± 0.02	25.50 ± 3.48	15.67 ± 1.36	9.47 ± 1.28
Bidirectional	0.46 ± 0.05	0.31 ± 0.03	0.18 ± 0.05	28.85 ± 3.23	30.73 ± 2.74	14.57 ± 2.88
Stationary	–	–	–	27.59 ± 4.18	34.73 ± 2.96	63.06 ± 3.87

Average speed of NPY-mCherry-labeled DCVs per neurite and directionality in human iPSC-derived neurons at DIV24 or DIV50 treated with nocodazole (Noc) or control (DMSO). n = 15–20 vesicles per neurite per micro-network. Twenty-four and 18 micro-networks from three independent inductions were analyzed for DIV50 and DIV24, respectively.

increase in SV secretion over time was found in neurons from a different iPSC line (Figures S6A–S6F). These data indicate that human iPSC-derived neurons at an early developmental stage (DIV22) contain SVs, which are acidic, and a few active synapses, but the vesicular pool is small and secretion efficiency is minimal. These parameters gradually increase over time until DIV50, but SV secretion efficiency remains lower than in mouse neurons.

DCV Secretion Efficiency Increases between DIV22 and DIV36 in Human iPSC-Derived Neurons

We next investigated whether DCV secretion efficiency follows the same developmental time course as SVs. From the earliest time point (DIV22) we observed punctate expression of NPY-mCherry (Figure 6A). The density of DCV puncta remained constant during development at a range of 0.30–0.35 puncta per μm, comparable with mouse neurons (Figures 6A and 6B). HFS (16 × 50 AP at 50 Hz) did not trigger efficient secretion at DIV22 as opposed to later time points (Figure 6C). DCV secretion efficiency, calculated as the number of DCV secretion events over the total number of DCV puncta, gradually increased over time until plateauing at DIV36, reaching a similar secretion efficiency as mouse neurons (~6%, Figure 6C). After DIV36, no significant increase in secretion efficiency was detected. Secretion preferentially occurred from stationary DCVs (~70%) over DCVs, stopping during HFS (Figure S7).

The distribution of DCV secretion events during HFS was similar at every developmental stage analyzed. This distribution was skewed, with approximately 20% of the events occurring during the first two bursts of stimulation, 50% during the first six bursts and almost 5% during the last two bursts. This was comparable with mouse neurons, where 30% of the events occurred during the first two bursts (Figures 6D and 6E; Farina et al., 2015). Similar secretion efficiency and kinetics were obtained from a second batch of human iPSC-derived neurons (Figures S6G–S6K).

Together, these results show that, while the density of DCVs remains constant, DCV secretion efficiency increases during development, reaching a plateau at DIV36 with a secretion efficiency similar to mouse neurons.

DISCUSSION

This study describes the maturation of the main secretory pathways in human iPSC-derived neurons. We developed standardized micro-network cultures that abundantly express endogenous SV and DCV markers, including neuropeptides, showing that DCV trafficking is similar to that previously observed in rodent neurons and that SV and DCV secretion is strictly calcium and SNARE dependent. Furthermore, we characterized the maturation of the two neurosecretory organelles, with DCVs reaching maximum secretion efficiency when that of SVs is still developing.

DCV Trafficking and Secretion Can be Studied at Single-Vesicle Resolution in Micro-networks of Human Neurons

The micro-networks of human iPSC-derived neurons described here express DCV markers in a punctate pattern

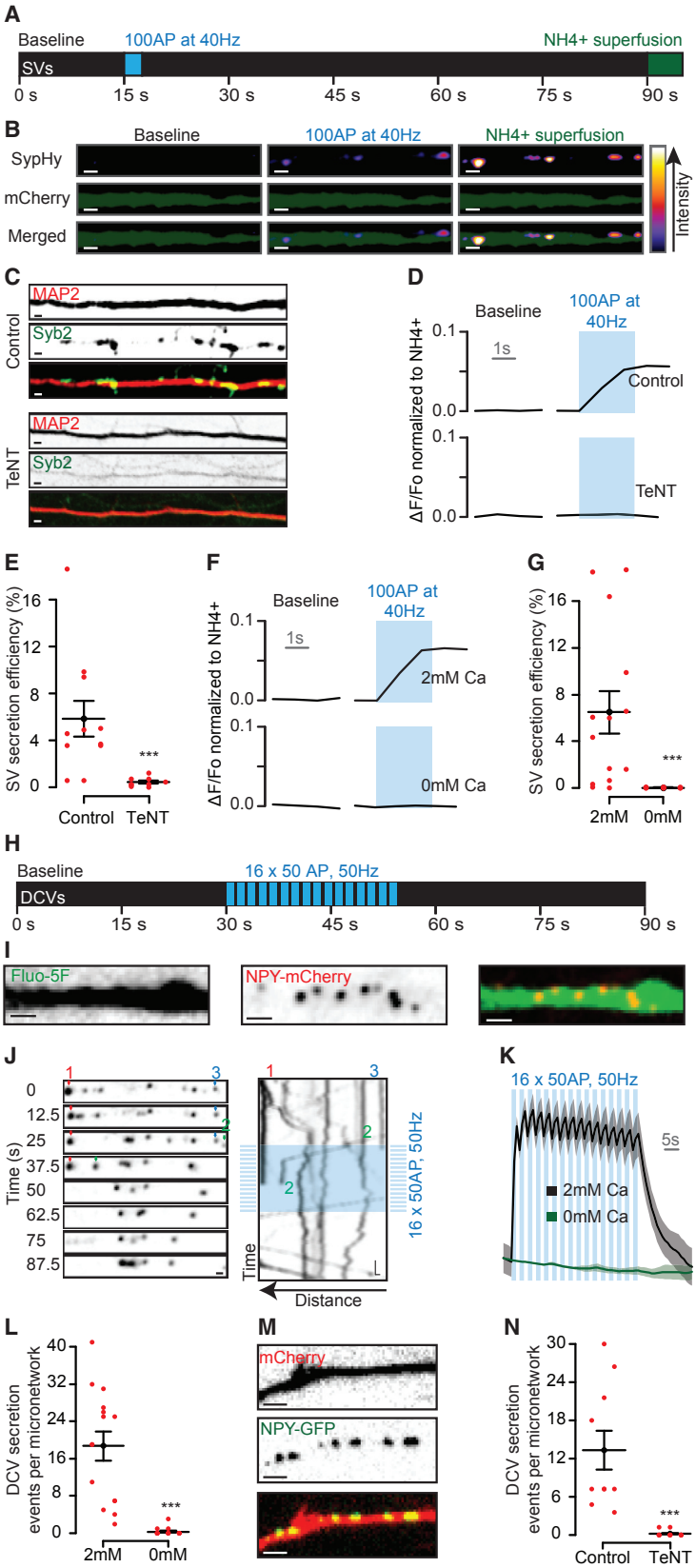

Figure 4. DCV and SV Secretion Is Calcium and SNARE Dependent in Human iPSC-Derived Neurons

(A) Diagram of SV secretion assay. After 15 s baseline, high-frequency stimulation (HFS; 100 AP at 40 Hz, blue bar) was applied to trigger secretion. NH_4^+ was superfused to estimate the vesicular pool.

(B) Representative neurites containing SypHy and soluble mCherry before and during HFS and after NH_4^+ superfusion. Intensity color code used for SypHy representation: black and white as lowest and highest, respectively.

(C) Representative examples of neurites expressing tetanus toxin (TeNT) (bottom) and control (top) immunostained for MAP2 and synaptobrevin-2 (Syb2).

(D and E) Average SypHy traces (D) and quantification (E) of SV secretion efficiency, calculated as SV secretion over NH_4^+ response, are reduced in TeNT-expressing human iPSC-derived neurons (control: 5.84% ± 1.55%, n = 11 cells; TeNT: 0.43% ± 0.13%, n = 10 cells; ***p = 3.6 × 10^{-4}, Mann-Whitney U test).

(F and G) Average SypHy traces (F) and quantification (G) of SV secretion efficiency, calculated as SV secretion over NH_4^+ response, are reduced in 0 mM extracellular calcium (2 mM: 6.49% ± 1.83%, n = 11 cells; 0 mM: 0.03% ± 0.01%, n = 10 cells; ***p = 4.55 × 10^{-5}, Mann-Whitney U test).

(H) Diagram of DCV secretion assay. After 30 s baseline, high frequency stimulation (HFS; 16 bursts of 50 AP at 50 Hz, blue bars) was applied to trigger secretion.

(I) Representative Fluo-5F-filled neurite containing NPY-mCherry puncta.

(J) Frames from time-lapse recording and corresponding kymograph showing dynamics and secretion of NPY-mCherry-labeled DCVs. Numbers indicate position of stationary vesicles (1, red; 3, blue) and a moving vesicle (2, green) that fused upon HFS.

(K) Intracellular calcium levels, measured with Fluo-5F, increase upon HFS in 2 mM but not in 0 mM extracellular calcium.

(L) DCV secretion is abolished in calcium-free external solution (2 mM Ca: 18.70 ± 3.12 events per micronetwork, n = 15; 0 mM Ca: 0.33 ± 0.21 events per micronetwork, n = 15; ***p = 1.93 × 10^{-6}, Mann-Whitney U test).

(M) Representative mCherry-filled neurite expressing NPY-GFP.

(N) DCV secretion is abolished in TeNT-expressing human iPSC-derived neurons (control: 11.10 ± 2.59 events per micro-network, n = 10 cells; TeNT: 0.13 ± 0.09 events per micro-network, n = 15, ***p = 7.9 × 10^{-6}, Mann-Whitney U test).

Bars show mean ± SEM. Bullets and columns represent individual observations and inductions, respectively. Scale bars, 2 μm (B), (C), (I), (M); 1 μm and 5 s (J). See also Figures S4 and S5.

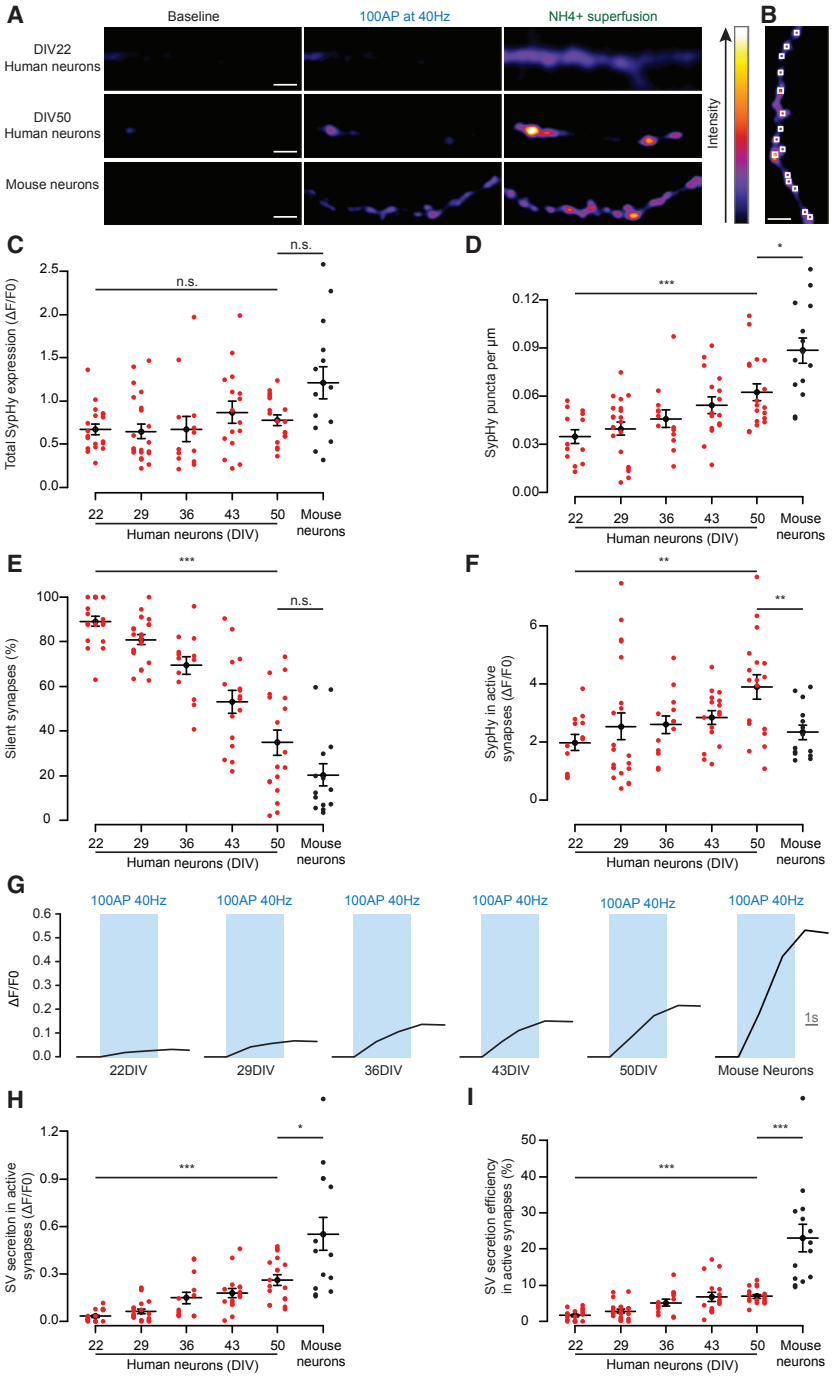

Figure 5. Synaptic Transmission Increases in Human iPSC-Derived Neurons from DIV22 to DIV50

(A and B) Representative neurites of SypHy-expressing human iPSC-derived neurons at DIV22 or DIV50 and mouse neurons before (left), during HFS (100 AP at 40 Hz, middle), and after $NH4^+$ (right). $NH4^+$ was superfused to visualize synapses and estimate the vesicular pool (B) (white squares). Intensity color-code used for SypHy representation: black and white as lowest and highest, respectively. Scale bars, 5 µm.

(C) Total SypHy expression, indicated by the average SypHy intensity, remains constant from DIV22 to DIV50 in human iPSC-derived neurons (DIV22: 0.62 ± 0.06 a.u.; DIV29: 0.65 ± 0.08 a.u.; DIV36: 0.68 ± 0.14 a.u.; DIV43: 0.87 ± 0.13 a.u.; DIV50: 0.84 ± 0.07 a.u., p = 0.087, linear regression [LR]) and similar to mouse neurons (1.27 ± 0.19 a.u., p = 0.084, Mann-Whitney U test [MW]).

(D) Density of SypHy puncta increases in human iPSC-derived neurons from DIV22 to DIV50 (DIV22: 0.035 ± 0.004 puncta per µm; DIV29: 0.040 ± 0.004 puncta per µm; DIV36: 0.046 ± 0.005 puncta per µm; DIV43: 0.054 ± 0.005 puncta per µm; DIV50: 0.062 ± 0.005 puncta per µm, ***p = 1.77 × 10^{-5}, LR) and remains below mouse neurons (0.088 ± 0.008 puncta per µm, *p = 0.011, MW).

(E) Percentage of silent synapses in human iPSC-derived neurons decreases from DIV22 to DIV50 (DIV22: 89.16% ± 2.35%; DIV29: 77.46% ± 2.18%; DIV36: 69.39% ± 4.03%; DIV43: 53.02% ± 5.16%; DIV50: 34.79% ± 5.57%, ***p = 2.0 × 10^{-16}, LR), reaching that of mouse neurons (20.29% ± 5.01%, p = 0.099, MW).

(F) SypHy intensity in active synapses of human iPSC-derived neurons increases from DIV22 to DIV50 (DIV22: 1.98 ± 0.27 a.u.; DIV29: 2.53 ± 0.47 a.u.; DIV36: 2.60 ± 0.31 a.u.; DIV43: 2.83 ± 0.24 a.u.; DIV50: 3.90 ± 0.41 a.u., **p = 0.002, LR) and surpasses that in mouse neurons (2.33 ± 0.24 a.u., **p = 0.003, MW).

(G) Average SypHy traces of SV secretion upon HFS (100 AP at 40 Hz, blue rectangles) in human iPSC-derived and mouse neurons.

(H) SV secretion in active synapses of human iPSC-derived neurons increases from DIV22 to DIV50 (DIV22: 0.03 ± 0.01 a.u.; DIV29: 0.07 ± 0.02 a.u.; DIV36: 0.15 ± 0.04 a.u.; DIV43: 0.18 ± 0.03 a.u.; DIV50: 0.26 ± 0.03 a.u., ***p = 1.84 × 10^{-13}, LR), but is lower than that in mouse neurons (0.55 ± 0.10 a.u., *p = 0.03, MW).

(I) Secretion efficiency of SVs in active synapses of human iPSC-derived neurons increases over time (DIV22: 1.65% ± 0.35%; DIV29: 2.93% ± 0.52%; DIV36: 5.14% ± 0.92%; DIV43: 6.76% ± 1.25%; DIV50: 6.96% ± 0.55%, ***p = 1.57× 10^{-10}, LR), but is lower than that in mouse neurons (22.56% ± 5.11%, ***p = 1.909 × 10^{-7}, MW).

Bars show mean ± SEM. Bullets and columns represent individual micro-networks and inductions (nests for mouse), respectively. LR was applied to human neurons. Mouse neurons were only tested against DIV50 human neurons using MW. n = 19 (DIV22), 22 (DIV29), 13 (DIV36), 16 (DIV43), 18 (DIV50), 14 (mouse neurons). Note that six recordings at DIV22 and one at DIV29 had no active synapses. See also Figure S6.

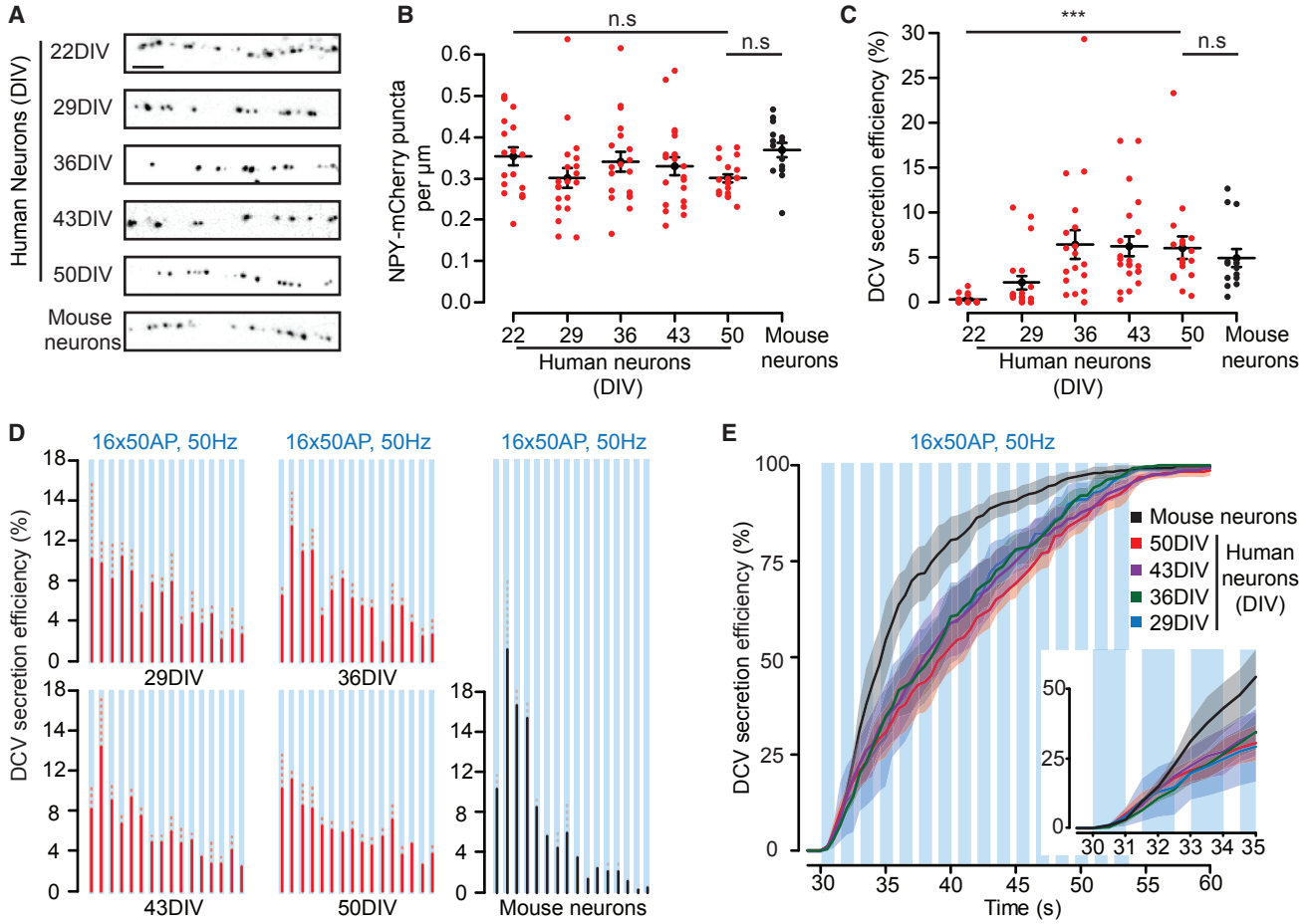

Figure 6. DCV Secretion Efficiency Increases in Human iPSC-Derived Neurons from DIV22 to DIV36

(A) Representative neurites of human iPSC-derived neurons at DIV22-DIV50 and mouse neurons expressing NPY-mCherry. Scale bar, 5 µm.

(B) Density of NPY-mCherry puncta remains constant in human iPSC-derived neurons from DIV22 to DIV50 (DIV22: 0.35 ± 0.02 puncta per µm; DIV29: 0.30 ± 0.02 puncta per µm; DIV36: 0.34 ± 0.02 puncta per µm; DIV43: 0.33 ± 0.02 puncta per µm; DIV50: 0.31 ± 0.01 puncta per µm, p = 0.276, LR) and similar to mouse neurons (0.34 ± 0.02 puncta per µm; p = 0.069, t test).

(C) Secretion efficiency of DCVs, calculated as DCV secretion events over total DCV pool, increases over time in human iPSC-derived neurons (DIV22: 0.29% ± 0.11%; DIV29: 2.18% ± 0.74%; DIV36: 6.42% ± 1.62%; DIV43: 6.24% ± 1.11%; DIV50: 6.06% ± 1.24%, ***p = 3.03×10^{-10}, LR), reaching a similar percentage as mouse neurons (4.94% ± 1.01%; p = 0.316, MW).

(D and E) Histogram (D) and cumulative plot (E) of DCV secretion events in human iPSC-derived neurons from DIV29 to DIV50 and mouse neurons. DIV22 not included due to low DCV secretion. Blue bars represent HFS (16 bursts of 50 AP at 50 Hz). Inset shows zoom of secretion during the first 4 bursts.

Bars show mean ± SEM. Bullets and columns represent individual micro-networks and inductions (nests for mouse), respectively. LR was applied to human neurons. Mouse neurons were only tested against DIV50 human neurons using MW or t test. n = 19 (DIV22), 20 (DIV29), 19 (DIV36), 21 (DIV43), 17 (DIV50), 14 (mouse neurons). See also Figures S6 and S7.

and DCVs were readily observed at the ultrastructural level. Expression of a cargo-reporter previously optimized in rodent neurons, NPY-mCherry (Farina et al., 2015; van de Bospoort et al., 2012), consistently yielded a punctate distribution that co-localized extensively (90%) with the endogenous DCV marker, CgB (Rosa et al., 1985), and had trafficking characteristics similar to rodents (see below). Furthermore, fusion of many individual DCVs was detected using the NPY-mCherry reporter upon bursts of APs in a strictly Ca^{2+}- and SNARE-dependent manner. A small percentage of the total reporter fluorescence did not co-localize with endogenous markers. This fluorescence may correspond to secreted NPY that remains attached to the membrane; NPY endocytosed after secretion or DCVs lacking CgB. Thirty percent of the CgB puncta did not contain reporter fluorescence. This fluorescence may correspond to older DCVs generated before expression of the reporter or to a limited differential sorting of cargos at the

Golgi. However, overall, NPY-mCherry is a suitable reporter to monitor DCV trafficking and secretion with single-vesicle resolution in micro-networks of human neurons.

DCV Trafficking and Secretion in Human Neurons Is Similar to Previously Observed Features in Rodents

As in other species, DCV trafficking relied on an intact microtubule cytoskeleton in human neurons. DCVs traveled in anterograde and retrograde directions and paused frequently. In axons, DCV trafficking was preferentially anterograde and faster than in dendrites, where there was no directional preference. Average axonal anterograde speed was 1 μm/s. These features are all in the same range as previously reported in rodents (de Wit et al., 2006; Kwinter et al., 2009). The different DCV dynamics between axons and dendrites may be explained by their different microtubule polarity (Baas et al., 1988) and/or the neurite-specific expression of microtubule-associated proteins that modulate trafficking (Dixit et al., 2008).

Bursts of APs triggered fusion of up to 40 DCVs per field of view, on average 6% of the total DCV pool at DIV36 and beyond. Such a (low) secretion efficiency is similar to that previously reported in mouse neurons (Farina et al., 2015; van de Bospoort et al., 2012), and is consistent with the generally accepted notion that DCV secretion requires intense stimulation (for a review, see Bartfai et al., 1988). The SNARE proteins synaptobrevin-2, SNAP25, and syntaxin1 were abundantly expressed in our micro-networks, and TeNT abolished DCV secretion, indicating the SNARE dependence of DCV secretion in human neurons, as shown before in rodents (de Wit et al., 2009; Shimojo et al., 2015). Finally, DCV secretion was, as in rodent neurons (de Wit et al., 2009; Farina et al., 2015; van de Bospoort et al., 2012), strictly Ca^{2+} dependent. Taken together, these features of DCV trafficking and secretion are very similar to those previously observed in rodent neurons, suggesting that similar mechanisms regulate these processes in rodent and human neurons, and that the culture system and fluorescent reporter optimized here, provide excellent tools to model human brain disorders related to DCV dysfunctions and test therapeutic targets on a patient-own background.

SV and DCV Secretory Pathways Mature Differentially in Human Neurons

Rodent synapses develop by recruiting SVs and increasing the concentration of pre- and postsynaptic proteins at the synapse (Chia et al., 2013; McAllister, 2007; Waites et al., 2005). Accordingly, we observed that, in human neurons, synaptic accumulations of SV markers, the fraction of active synapses, and the amount of SV secretion all developed progressively until DIV50. However, these parameters remained lower than DIV14 mouse hippocampal neurons. It was not possible to maintain micro-networks much longer than DIV50 due to deterioration of the underlying glia feeders (data not shown), and it remains unknown whether further maturation would have produced levels similar to rodent neurons. In contrast, SypHy expression in active synapses of human neurons was higher than mouse neurons, suggesting that human synapses may contain more SVs per synapse or more SypHy per SV.

As opposed to the SV secretory pathway, the DCV pathway acquired maximum secretion efficiency at a relatively early developmental stage (DIV36), with DCV fusion kinetics and density remaining constant throughout subsequent stages and being similar to mature rodent neurons (Farina et al., 2015; van de Bospoort et al., 2012). Hence, development of DCV secretion efficiency preceded that of SVs. While maturation of synaptic transmission is relatively well documented (McAllister, 2007; Waites et al., 2005), little systematic information is available so far on the maturation of the DCV secretory pathway. DCVs bud off from the TGN where cargo is sorted between regulated (DCV) and constitutive secretory pathways and between axonal and dendritic destinations, by largely unknown mechanisms (Dikeakos and Reudelhuber, 2007; Maday et al., 2014). Developing rodent neurons are known to express and use DCVs early in their development: guidance cues required for network formation and synaptogenesis are targeted to the surface of the cell using regulated DCV secretion (de Wit et al., 2006; de Wit et al., 2009), TGN-derived vesicles are targeted to the future axons during initial axogenesis (Bradke and Dotti, 1997), active zone components are targeted to future synapses in TGN-derived vesicles with dense cores and a similar diameter as DCVs (referred to as PTVs, Zhai et al., 2001), and trophic factors are secreted from DCVs to promote synapse maturation (Gottmann et al., 2009). These observations indicate that the DCV secretory pathway indeed matures before the SV pathway and might even be required for the SV pathway to develop fully (Shapira et al., 2003; Zhai et al., 2001). Considerable heterogeneity appears to exist within the DCV secretory pathway. DCV-like organelles probably contain different cargo types during different phases of neuronal development (guidance cues, active zone constituents, trophic factors, neuropeptides), and these different populations of organelles may mature differently. However, our DCV cargo-reporter approach samples DCV trafficking and fusion efficiency during all these phases and therefore we can demonstrate the maturation time course of the DCV pathway relative to the SV pathway and show, in a side-by-side comparison, that while DCV secretion has reached its maximum capacity SV secretion capacity is still minimal.

SV secretion in human neurons has been reported by several recent studies. However, most of these studies only report spontaneous fusion of SVs, the biological

significance of which is unclear and, with a few exceptions (such as Chanda et al., 2014; Sun et al., 2016; Yi et al., 2016; Zhang et al., 2013), these studies do not demonstrate action potential-evoked secretion, which is the basis for synaptic transmission. Thus, it cannot be excluded that some of these studies are sampling from rather immature synapses given that spontaneous fusion of SVs per se is not sufficient to conclude that synapses are mature. This may influence the interpretation of certain findings in relation to human disease of the adult or aging brain. Robust evoked postsynaptic currents or evoked increases in SypHy fluorescence, as demonstrated here, are a prerequisite for the correct interpretation of synaptic defects in relation to human disease.

EXPERIMENTAL PROCEDURES

Primary Mouse Neurons Culture

As described previously (de Wit et al., 2009), hippocampi were dissected from embryonic day 18.5 mouse embryos in Hank's balanced salt solution (Sigma), digested in 0.25% trypsin (Life Technologies) for 20 min at 37°C and dissociated with fire-polished Pasteur pipettes. Dissociated neurons were resuspended in supplemented Neurobasal (see Supplemental Information) and plated on the astrocyte micro-network (1,500 neurons/well). Neurons were maintained at 37°C and 5% CO_2 for 14 days.

Agarose-coated glass coverslips stamped with a 0.1 mg/mL poly-D-lysine (Sigma) and 0.7 mg/mL rat tail collagen (BD Biosciences) mixture were used for micro-network (Mennerick et al., 1995) as described previously (Wierda et al., 2007). Six thousand rat glia cells were plated per coverslip.

Animals were housed and bred according to institutional and Dutch guidelines.

Human iPSC-Derived Neurons Culture

Neuroepithelial stem cells (NESCs) were generated from two independent iPSC lines (hVS-88 and hVS-60). Only NESCs from a low-number passage (1–4) were used for subsequent differentiations, using 1.8 μM of the Shh agonist purmorphamine (Cayman Chemical) and 10 μM valproic acid (Sigma) for 4 and 3 days, respectively (Ma et al., 2012). After 8 days, cells were digested in Accutase (Millipore) and re-plated in a 1:2 ratio on PLO-laminin-coated plates. At DIV17, neurons were re-plated on astrocyte-supported micro-networks (5,000 neurons/well) or UV-sterilized glass coverslips (50,000 neurons/well) coated with poly-L-ornithine (PLO, Sigma) and laminin (Sigma). To stop cell proliferation, 2 μM AraC (Sigma) was added for 24 hr. Glia support was increased by placing coverslips in close proximity to astrocytes previously grown on the bottom of 12-well plates (Kaech and Banker, 2006). Cultures were maintained at 37°C and 5% CO_2 in supplemented Neurobasal (see Supplemental Information) with growth factor (20 ng/μL brain-derived neurotrophic factor [PeproTech], 10 ng/mL glial cell-derived neurotrophic factor [PeproTech], 10 ng/mL insulin growth factor 1 [PeproTech], and 1 μM cAMP [Sigma]). Cultures were half-fed every 3.5 days.

Plasmids

NPY-mCherry (de Wit et al., 2009; Farina et al., 2015), synaptophysin-pHluorin (Granseth et al., 2006), and TeNT, engineered as TeNT-IRES-mCherry, were cloned into pLenti vectors under the control of a human synapsin promoter.

Immunocytochemistry

Neurons were fixed with 3.7% paraformaldehyde (Electron Microscopy Sciences) in PBS for 20 min at room temperature (RT) and permeabilized with 0.5% Triton X for 5 min. Blocked with 2% normal goat serum (Life Technologies), 0.1% Triton X (Fisher Scientific) for 20 min at RT. Incubation with primary (see Supplemental Information) and secondary antibodies was done at RT for 2 or 1 hr, respectively. Coverslips were mounted in Mowiol and imaged in a confocal microscope (Nikon Eclipse Ti) equipped with 10× (numerical aperture [NA] = 0.45) and 63× oil (NA = 1.40) objectives controlled by NisElements 4.30 software.

Live Imaging

Coverslips were placed in an imaging chamber and perfused with Tyrode's buffer (composition in mM: 2 $CaCl_2$, 2.5 KCl, 119 NaCl, 2 $MgCl_2$, 20 glucose, and 25 HEPES [pH 7.4]). Recordings were done at 32°C–34°C using an AxioObserver.Z1 microscope (Zeiss) with laser-based illumination (488 and 561 nm), appropriate filter sets, 40× oil objective (NA = 1.3) and an electron microscopy (EM) charge-coupled device camera (Hamamatsu). Time-lapse recordings were acquired using Axiovision 4.8 at 1 Hz (for SV secretion) or 2 Hz (for DCV trafficking and secretion) with 100 ms exposure. HFS was applied using parallel platinum electrodes delivering 30 mA, 1 ms pulses controlled by a Master-8 (AMPI) and a stimulus generator (A365, WPI). Intracellular pH was neutralized with Tyrode's solution in which 50 mM NaCl was replaced by 50 mM NH_4Cl applied by gravity flow through a glass capillary placed between the platinum electrodes. In calcium-free experiments, $CaCl_2$ was substituted for 4 mM $MgCl_2$ and 5 mM EGTA.

Incubation with 2 μM Fluo-5F AM (Molecular Probes) or 10 μM nocodazole (Tocris) (in 0.1% DMSO) was done at 37°C and 5% CO_2 for 10 and 45 min, respectively. During image acquisition, neurons were perfused with Tyrode's containing nocodazole/DMSO or only DMSO.

Image Analysis

Traces were expressed as fluorescence change (ΔF) over initial fluorescence (F0, obtained by averaging the first ten frames of the time-lapse recording). All non-mobile SypHy puncta with a fluorescence increase of >3 SD upon NH_4^+ superfusion were considered synapses. Synapses with a fluorescence increase of >3 SD upon stimulation were considered active. NPY-mCherry puncta disappearing from a 3 × 3 pixel region of interest were counted as DCV secretion events. Neurites were classified as dendrites or axons if the diameter was >1.5 or <1 μm, respectively. Secretion also occurred in regions were the density of neurites was too high to bona-fide classify secretion as axonal or dendritic, therefore secretion was only analyzed as events per micro-network. For DCV trafficking, random stretches of neurites containing 15–20 clearly distinguishable puncta per stretch were analyzed. Only neurites that could be clearly classified as dendrites or axons and traced back to the soma

were included. Puncta was considered anterograde or retrograde if they moved away or toward the soma, respectively. Stationary puncta moved ≤0.6 μm during the recording. Puncta were considered to pause when moved ≤0.6 μm for at least 5 s.

Synapses and DCV puncta were analyzed with SynD software (Schmitz et al., 2011) using MAP2 or Fluo-5F as a morphology mask. Mander's and Pearson's coefficients were used for co-localization analysis (JACOP, ImageJ, default threshold).

Electron Microscopy

Neurons were fixed for 90 min at RT with 2.5% glutaraldehyde in 0.1 M cacodylate buffer (pH 7.4). Cells were washed and post-fixed for 1 hr at RT with 1% OsO_4/1% $KRu(CN)_6$. After dehydration through a series of increasing ethanol concentrations, cells were embedded in Epon and polymerized for 48 hr at 60°C. Ultrathin sections (80 nm) were cut parallel to the cell monolayer, collected on single-slot Formvar-coated copper grids, and stained in uranyl acetate and lead citrate in a Leica EM AC20 Ultra stainer. Neuronal sections were randomly selected at low magnification and photographed at 80k magnification using a JEOL1010 transmission electron microscope at 60 kV.

Statistics

Shapiro and Levene's tests were used to test distribution normality and homogeneity of variances, respectively. When assumptions of normality or homogeneity of variances were met, parametric tests were used: t test or one-way ANOVA (Tukey as post hoc). Otherwise, non-parametric tests were used: Mann-Whitney U or Kruskal-Wallis test (Holm as post hoc). Linear regression was used for development studies with square transformations when data was not normally distributed. R was used as software.

SUPPLEMENTAL INFORMATION

Supplemental Information includes Supplemental Experimental Procedures, seven figures, and three movies and can be found with this article online at http://dx.doi.org/10.1016/j.stemcr.2017.01.019.

AUTHOR CONTRIBUTIONS

J.E.M., R.F.T., and M.V. designed the experiments. J.E.M. collected and analyzed live and confocal imaging data. J.vW. collected and analyzed electron microscopy data. A.G.N. differentiated iPSCs to NESCs supervised by V.H. D.S. generated micro-networks of human iPSC-derived neurons and mouse neurons. J.E.M., R.F.T., and M.V. designed figures and wrote the manuscript with input from all authors.

ACKNOWLEDGMENTS

The authors thank Robbert Zalm for cloning and producing viral particles, Frank den Oudsten for producing glia feeders, Rien Dekker for expert assistance in electron microscopy, and members of the CNCR iPSC project team for fruitful discussions. This work is supported by a Proof-of-Concept fund from the Neuroscience Campus Amsterdam (to V.H. and M.V.) and by an ERC Advanced Grant (322966) from the European Union (to M.V.).

Received: October 11, 2016
Revised: January 22, 2017
Accepted: January 23, 2017
Published: February 23, 2017

REFERENCES

Allen, Y.S., Adrian, T.E., Allen, J.M., Tatemoto, K., Crow, T.J., Bloom, S.R., and Polak, J.M. (1983). Neuropeptide Y distribution in the rat brain. Science *221*, 877–879.

Baas, P.W., Deitch, J.S., Black, M.M., and Banker, G.A. (1988). Polarity orientation of microtubules in hippocampal neurons: uniformity in the axon and nonuniformity in the dendrite. Proc. Natl. Acad. Sci. USA *85*, 8335–8339.

Bartfai, T., Iverfeldt, K., Fisone, G., and Serfozo, P. (1988). Regulation of the release of coexisting neurotransmitters. Annu. Rev. Pharmacol. Toxicol. *28*, 285–310.

Bradke, F., and Dotti, C.G. (1997). Neuronal polarity: vectorial cytoplasmic flow precedes axon formation. Neuron *19*, 1175–1186.

Chanda, S., Ang, C.E., Davila, J., Pak, C., Mall, M., Lee, Q.Y., Ahlenius, H., Jung, S.W., Sudhof, T.C., and Wernig, M. (2014). Generation of induced neuronal cells by the single reprogramming factor ASCL1. Stem Cell Rep. *3*, 282–296.

Chia, P.H., Li, P., and Shen, K. (2013). Cell biology in neuroscience: cellular and molecular mechanisms underlying presynapse formation. J. Cell Biol. *203*, 11–22.

de Wit, J., Toonen, R.F., Verhaagen, J., and Verhage, M. (2006). Vesicular trafficking of semaphorin 3A is activity-dependent and differs between axons and dendrites. Traffic *7*, 1060–1077.

de Wit, J., Toonen, R.F., and Verhage, M. (2009). Matrix-dependent local retention of secretory vesicle cargo in cortical neurons. J. Neurosci. *29*, 23–37.

Dikeakos, J.D., and Reudelhuber, T.L. (2007). Sending proteins to dense core secretory granules: still a lot to sort out. J. Cell Biol. *177*, 191–196.

Dixit, R., Ross, J.L., Goldman, Y.E., and Holzbaur, E.L. (2008). Differential regulation of dynein and kinesin motor proteins by tau. Science *319*, 1086–1089.

Farina, M., van de Bospoort, R., He, E., Persoon, C.M., van Weering, J.R., Broeke, J.H., Verhage, M., and Toonen, R.F. (2015). CAPS-1 promotes fusion competence of stationary dense-core vesicles in presynaptic terminals of mammalian neurons. Elife *4*, e12968.

Gottmann, K., Mittmann, T., and Lessmann, V. (2009). BDNF signaling in the formation, maturation and plasticity of glutamatergic and GABAergic synapses. Exp. Brain Res. *199*, 203–234.

Granseth, B., Odermatt, B., Royle, S.J., and Lagnado, L. (2006). Clathrin-mediated endocytosis is the dominant mechanism of vesicle retrieval at hippocampal synapses. Neuron *51*, 773–786.

Hirokawa, N., Niwa, S., and Tanaka, Y. (2010). Molecular motors in neurons: transport mechanisms and roles in brain function, development, and disease. Neuron *68*, 610–638.

Hook, V., Brennand, K.J., Kim, Y., Toneff, T., Funkelstein, L., Lee, K.C., Ziegler, M., and Gage, F.H. (2014). Human iPSC neurons display activity-dependent neurotransmitter secretion: aberrant

catecholamine levels in schizophrenia neurons. Stem cell Rep. *3*, 531–538.

Huang, E.J., and Reichardt, L.F. (2001). Neurotrophins: roles in neuronal development and function. Annu. Rev. Neurosci. *24*, 677–736.

Ichida, J.K., and Kiskinis, E. (2015). Probing disorders of the nervous system using reprogramming approaches. EMBO J. *34*, 1456–1477.

Kaech, S., and Banker, G. (2006). Culturing hippocampal neurons. Nat. Protoc. *1*, 2406–2415.

Kaeser, P.S., and Regehr, W.G. (2014). Molecular mechanisms for synchronous, asynchronous, and spontaneous neurotransmitter release. Annu. Rev. Physiol. *76*, 333–363.

Kim, T., Gondre-Lewis, M.C., Arnaoutova, I., and Loh, Y.P. (2006). Dense-core secretory granule biogenesis. Physiology *21*, 124–133.

Kwinter, D.M., Lo, K., Mafi, P., and Silverman, M.A. (2009). Dynactin regulates bidirectional transport of dense-core vesicles in the axon and dendrites of cultured hippocampal neurons. Neuroscience *162*, 1001–1010.

Ma, L., Hu, B., Liu, Y., Vermilyea, S.C., Liu, H., Gao, L., Sun, Y., Zhang, X., and Zhang, S.C. (2012). Human embryonic stem cell-derived GABA neurons correct locomotion deficits in quinolinic acid-lesioned mice. Cell stem Cell *10*, 455–464.

Maday, S., Twelvetrees, A.E., Moughamian, A.J., and Holzbaur, E.L. (2014). Axonal transport: cargo-specific mechanisms of motility and regulation. Neuron *84*, 292–309.

Maeder, C.I., Shen, K., and Hoogenraad, C.C. (2014). Axon and dendritic trafficking. Curr. Opin. Neurobiol. *27*, 165–170.

McAllister, A.K. (2007). Dynamic aspects of CNS synapse formation. Annu. Rev. Neurosci. *30*, 425–450.

Mennerick, S., Que, J., Benz, A., and Zorumski, C.F. (1995). Passive and synaptic properties of hippocampal neurons grown in microcultures and in mass cultures. J. Neurophysiol. *73*, 320–332.

Merkle, F.T., Maroof, A., Wataya, T., Sasai, Y., Studer, L., Eggan, K., and Schier, A.F. (2015). Generation of neuropeptidergic hypothalamic neurons from human pluripotent stem cells. Development *142*, 633–643.

Meyer-Lindenberg, A., Domes, G., Kirsch, P., and Heinrichs, M. (2011). Oxytocin and vasopressin in the human brain: social neuropeptides for translational medicine. Nat. Rev. Neurosci. *12*, 524–538.

Park, H., and Poo, M.M. (2013). Neurotrophin regulation of neural circuit development and function. Nat. Rev. Neurosci. *14*, 7–23.

Rizo, J., and Sudhof, T.C. (2012). The membrane fusion enigma: SNAREs, Sec1/Munc18 proteins, and their accomplices–guilty as charged? Annu. Rev. Cell Dev. Biol. *28*, 279–308.

Rosa, P., Hille, A., Lee, R.W., Zanini, A., De Camilli, P., and Huttner, W.B. (1985). Secretogranins I and II: two tyrosine-sulfated secretory proteins common to a variety of cells secreting peptides by the regulated pathway. J. Cell Biol. *101*, 1999–2011.

Sah, R., and Geracioti, T.D. (2013). Neuropeptide Y and posttraumatic stress disorder. Mol. Psychiatry *18*, 646–655.

Schmitz, S.K., Hjorth, J.J., Joemai, R.M., Wijntjes, R., Eijgenraam, S., de Bruijn, P., Georgiou, C., de Jong, A.P., van Ooyen, A., Verhage, M., et al. (2011). Automated analysis of neuronal morphology, synapse number and synaptic recruitment. J. Neurosci. Methods *195*, 185–193.

Shapira, M., Zhai, R.G., Dresbach, T., Bresler, T., Torres, V.I., Gundelfinger, E.D., Ziv, N.E., and Garner, C.C. (2003). Unitary assembly of presynaptic active zones from Piccolo-Bassoon transport vesicles. Neuron *38*, 237–252.

Shimojo, M., Courchet, J., Pieraut, S., Torabi-Rander, N., Sando, R., 3rd, Polleux, F., and Maximov, A. (2015). SNAREs controlling vesicular release of BDNF and development of callosal axons. Cell Rep. *11*, 1054–1066.

Sudhof, T.C., and Rothman, J.E. (2009). Membrane fusion: grappling with SNARE and SM proteins. Science *323*, 474–477.

Sun, Y., Pasca, S.P., Portmann, T., Goold, C., Worringer, K.A., Guan, W., Chan, K.C., Gai, H., Vogt, D., Chen, Y.J., et al. (2016). A deleterious Nav1.1 mutation selectively impairs telencephalic inhibitory neurons derived from Dravet syndrome patients. Elife *5*. http://dx.doi.org/10.7554/eLife.13073.

Vale, R.D. (2003). The molecular motor toolbox for intracellular transport. Cell *112*, 467–480.

van de Bospoort, R., Farina, M., Schmitz, S.K., de Jong, A., de Wit, H., Verhage, M., and Toonen, R.F. (2012). Munc13 controls the location and efficiency of dense-core vesicle release in neurons. J. Cell Biol. *199*, 883–891.

van den Pol, A.N. (2012). Neuropeptide transmission in brain circuits. Neuron *76*, 98–115.

Volk, L., Chiu, S.L., Sharma, K., and Huganir, R.L. (2015). Glutamate synapses in human cognitive disorders. Annu. Rev. Neurosci. *38*, 127–149.

Waites, C.L., Craig, A.M., and Garner, C.C. (2005). Mechanisms of vertebrate synaptogenesis. Annu. Rev. Neurosci. *28*, 251–274.

Wierda, K.D., Toonen, R.F., de Wit, H., Brussaard, A.B., and Verhage, M. (2007). Interdependence of PKC-dependent and PKC-independent pathways for presynaptic plasticity. Neuron *54*, 275–290.

Yi, F., Danko, T., Botelho, S.C., Patzke, C., Pak, C., Wernig, M., and Sudhof, T.C. (2016). Autism-associated SHANK3 haploinsufficiency causes Ih channelopathy in human neurons. Science *352*, aaf2669.

Zaben, M.J., and Gray, W.P. (2013). Neuropeptides and hippocampal neurogenesis. Neuropeptides *47*, 431–438.

Zhai, R.G., Vardinon-Friedman, H., Cases-Langhoff, C., Becker, B., Gundelfinger, E.D., Ziv, N.E., and Garner, C.C. (2001). Assembling the presynaptic active zone: a characterization of an active one precursor vesicle. Neuron *29*, 131–143.

Zhang, Y., Pak, C., Han, Y., Ahlenius, H., Zhang, Z., Chanda, S., Marro, S., Patzke, C., Acuna, C., Covy, J., et al. (2013). Rapid single-step induction of functional neurons from human pluripotent stem cells. Neuron *78*, 785–798.